



Article

Structural Characteristics of Endorheic Rivers in the Tarim Basin

Yichu Wang¹ , Danlu Liu², Enhang Liang² and Jinren Ni^{2,*} ¹ College of Water Sciences, Beijing Normal University, Beijing 100875, China² The Key Laboratory of Water and Sediment Sciences, Ministry of Education, College of Environmental Sciences and Engineering, Peking University, Beijing 100871, China

* Correspondence: jinrenni@pku.edu.cn; Tel.: +86-10-62751185

Abstract: Endorheic rivers as landlocked systems with no hydrological connections to marine environments are suffering from water and ecosystem crisis worldwide, yet little is known about their structural characteristics with complex geomorphic and climatic dependence. Based on the river networks identified from 30 m resolution digital elevation models and surface water dynamic information derived from Landsat images, we investigate the hierarchical characteristics of 60 sub-basins in the Tarim Basin, the largest endorheic river basin in China. In the Tarim River basin, endorheic rivers exhibit a self-similarity only in the range of stream-orders 1–4, compared to the range of stream-orders 1–5 observed in exorheic rivers, owing to the limited stream power to maintain the similar aggregation of rivers in the arid regions. Moreover, the Tarim River networks demonstrate lower bifurcation ratio (2.48), length ratio (2.03), fractal dimension (1.38), and drainage density (0.24 km^{-1}) in representative sub-basins, with a significant decay in median values compared with those derived from exorheic rivers at similar scales, suggesting sparser and imperfect developed branching river networks in endorheic basins. Further analysis on the Tarim reveals that endorheic river structure is more related to glacier extent ($r = 0.67\sim 0.84$), potential evapotranspiration ($r = 0.63\sim 0.81$), and groundwater type index ($r = 0.64\sim 0.73$), which is essentially different from the structure of exorheic river represented by the Yellow River largely controlled by surface runoff, precipitation, and vegetation coverage. This study stresses the differences in intrinsic structural characteristics and extrinsic drivers of endorheic and exorheic rivers and highlights the necessity of differentiated strategies for endorheic river management in fragile ecosystems.

Keywords: endorheic river; self-similarity; structural characteristic; river-basin relation; Tarim

Citation: Wang, Y.; Liu, D.; Liang, E.; Ni, J. Structural Characteristics of Endorheic Rivers in the Tarim Basin. *Remote Sens.* **2022**, *14*, 4502. <https://doi.org/10.3390/rs14184502>

Academic Editors: Senthilnath Jayavelu, Shengli Tao and Xuesong Zhang

Received: 15 August 2022

Accepted: 5 September 2022

Published: 9 September 2022

Publisher's Note: MDPI stays neutral with regard to jurisdictional claims in published maps and institutional affiliations.



Copyright: © 2022 by the authors. Licensee MDPI, Basel, Switzerland. This article is an open access article distributed under the terms and conditions of the Creative Commons Attribution (CC BY) license (<https://creativecommons.org/licenses/by/4.0/>).

1. Introduction

Endorheic rivers play an important role in water resources allocation [1], carbon cycle [2], biodiversity [3], and socio-economic development [4] in arid regions. Unlike exorheic river systems with good hydrological connections to marine environments, endorheic rivers as landlocked fragile eco-environmental systems are facing a crisis of drying out of rivers [5,6], loss of channel connectivity [7,8], decline in water storage [9], and depletion of groundwater [10] worldwide, which further lead to increased droughts frequency, land degradation, damaged ecological integrity, and biodiversity loss under climate change and human interventions [11,12].

As the product of the arid and semi-arid climate, endorheic rivers exhibit particular characteristics in both river structures and basin properties. The endorheic river systems are usually composed of middle and small rivers with ephemeral flows [7]. Lacking sufficient flow energy to erode through the topographic barriers, the rivers converge to the inside of the basin, known as a 'sink', which may be permanent or ephemeral lakes, swamp, or even desert [13]. The drainage pattern of endorheic rivers is more likely to be radial as rivers converge into a lake and organize as more parallel when the sink is a salt flat or

desert. Due to limited precipitation and extremely strong evaporation [14], the endorheic rivers are unable to develop into dendritic networks that are common in the exorheic rivers. Moreover, the endorheic river networks usually show a temporal pattern of expansion and contraction [15], characterized with intermittent streamflow and ephemeral channels [16].

Endorheic rivers show more complicated hydrologic, geomorphologic, and hydrogeologic conditions than exorheic rivers [17]. The elevation of a 'sink' is usually local minima in the endorheic river basin; thus, the landlocked river basin acts as a depression topographically [18–20]. Consequently, most endorheic river systems have independent hydrological cycle within the basin. Diverse surface underlying types, such as glacier, oasis, grass, lake, wetland, and desert, are widely distributed in the endorheic river basins [21,22], which strongly influence the infiltration and interception processes [17]. The upper-stream part (e.g., mountain area) of endorheic basins are mainly supplied by snowmelt of glacier and precipitation, while the middle and lower stream parts are always primarily supplied by groundwater [23,24]. In particular, the gains and losses of groundwater, which are controlled by hydrogeological features and geological transitions along the channel, play a very important role in providing moisture for both the surface and subsurface [25], considering the short duration of overland flow from storm events in the endorheic regions.

Currently, exorheic rivers have been explored by coupling primary basin factors, such as precipitation, topography, underlying rocks, soil, and vegetation [26–28], under climate change and human interference [29,30]. With the unique river networks and complex basin properties, the relationship between river structure and basin factors of endorheic rivers would be quite different from exorheic rivers. However, existing studies on characteristics of endorheic rivers mainly focus on watershed delineation [18,19], streamflow dynamics [7], water storage variation [5,9], geomorphology characterization [31,32], and material circulation [2,33] as well as ecological health [34,35]. In 2013, Dorsaz et al. [13] made a quantitative analysis of the three endorheic river basins in Chile in terms of descriptors such as Horton's ratios, drainage density, and normalized Euclidean length, and indicated differences in river networks between exorheic and endorheic rivers.

Noting the insufficient understandings on characteristics of endorheic rivers and their geomorphic and climatic dependence, we investigate the structures of river networks in 60 representative sub-basins of the Tarim River basin, the largest endorheic river basin in China. With a comparison between the Tarim and the Yellow River basin, we elucidated the significant difference in stream-order range of self-similarity, structural characteristics, and influencing factors of endorheic and exorheic rivers, which is helpful to decision making for river management in vulnerable ecosystems.

2. Materials and Methods

2.1. Study Area

As the largest endorheic basin in China, the Tarim River basin (Figure 1) is distributed in 73°28'E–93°25'E and 34°40'N–43°20'N, with a total area of 1.02×10^6 km². The Tarim River is highly dependent on the water source from the TienShan, Kunlun, Eastern Pamir, and Karakorum mountains that surround the basin, with violent evaporation [36]. Under the extreme arid climate, the mean annual precipitation of Tarim is 116.8 mm. Peak flow months in the rivers are July, August, and September, which are influenced by snow melting and glacier melting [24]. Major rivers, such as the Tarim River, Hotan River, Keriya River, and Qarqan River, are intermittent rivers with streamflow usually occurring during June~September [24]. The shortage of water resources and fragility of ecological environment are two key constraints for sustainable river management as well as regional economic development in the Tarim Basin [8].

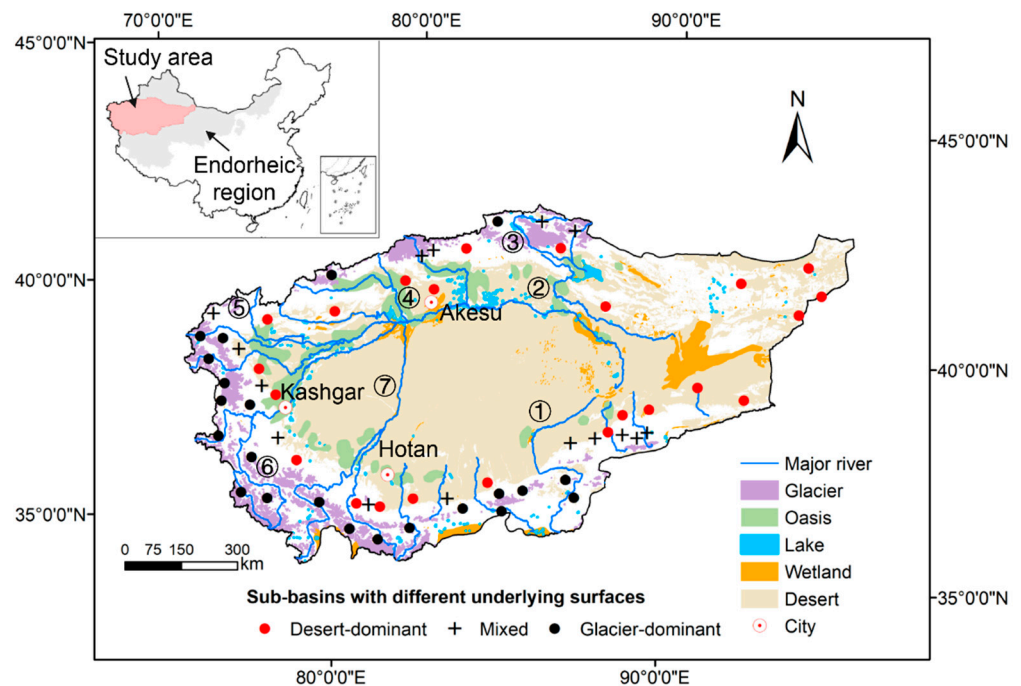


Figure 1. Study area. Location of representative sub-basins with different underlying surface conditions in the Tarim River basin. ①–⑦ refer to major rivers in the study area, correspondingly named Qarqan River, Tarim River, Kaidu River, Aksu River, Kashgar River, Yarkant River, and Hotan River.

We selected 60 sub-basins in the Tarim River basin with different climatic and geomorphic conditions (Figure 1). The catchment areas of these 60 sub-basins range from 1049 km² to 22,533 km², and the maximum Strahler orders range from 6 to 7.

2.2. Data Sources

Digital elevation modes (DEMs) at 30 m × 30 m resolution for extraction of river networks and basin boundaries are available at <https://search.earthdata.nasa.gov/search> (accessed on 31 December 2011).

The HydroSHEDS, HydroLakes, and HydroBASINS data databases at 15 arc-second resolution for initial sink locating and basin boundary delineation were accessed at <https://hydrosheds.org/> (accessed on 30 April 2022). Global wetland and lake datasets (GWLD) were obtained via <http://www.wwfus.org/science/data.cfm> (accessed on 1 July 2020). Water occurrence data [37] for modification of extracted drainage networks were accessible via <http://global-surface-water.appspot.com> (accessed on 31 December 2016). The referenced river networks data of the partial endorheic rivers for validation were collected from <http://www.resdc.cn/> (accessed on 31 December 2005). Precipitation and temperature data were assessed via <https://www.worldclim.org/> (accessed on 31 January 2020). Land surface runoff data were obtained from <http://www.bafg.de/grdc.htm> (accessed on 28 August 2008). Actual evapotranspiration and soil water content data were obtained from Global High-Resolution Soil-Water Balance dataset (<https://doi.org/10.6084/m9.figshare.7707605.v3>, accessed on 2 December 2019). Potential evapotranspiration and aridity index data (30 arc-seconds) for the years 1970–2000 were download from the <https://doi.org/10.6084/m9.figshare.7504448.v3> (accessed on 18 January 2019). Information on groundwater type data was extracted from the hydrogeological map via <https://geocloud.cgs.gov.cn/> (accessed on 31 October 2020). Datasets of landform type, soil type, and vegetation type at 1:1 million spatial resolutions were provided by Data Center for Resources and Environmental Sciences, Chinese Academy of Sciences (<http://www.resdc.cn>, accessed on 31 May 2001), and National Cryosphere Desert Data Center (<http://www.ncdc.ac.cn/portal/>, accessed on 31 October 2019).

2.3. Identification of Hierarchical Endorheic Rivers

As is well known, the accuracy of river networks and watershed boundaries are closely related to DEMs resolution [38,39], adopted algorithms [40–42], and local basin conditions. In this study, we identified endorheic river networks from 30 m resolution DEMs because relatively large-scale basins like the Tarim River basin and its sub-basins are more concerned instead of the details in a small endorheic river basin. The advances in extraction of river networks have been made by developing optimized algorithms related to DEMs pretreatment, flow direction determination, and channel identification, as well as efficiency upgradation. For endorheic rivers eventually flowing to lakes or deserts, both the depression topography and insufficient streamflow in endorheic river basin limit the accurate identification of channels through DEM. Hence, we established a framework for identification of endorheic rivers and basin boundaries composed with three modules (I, II, III), which are shown in Figure 2.

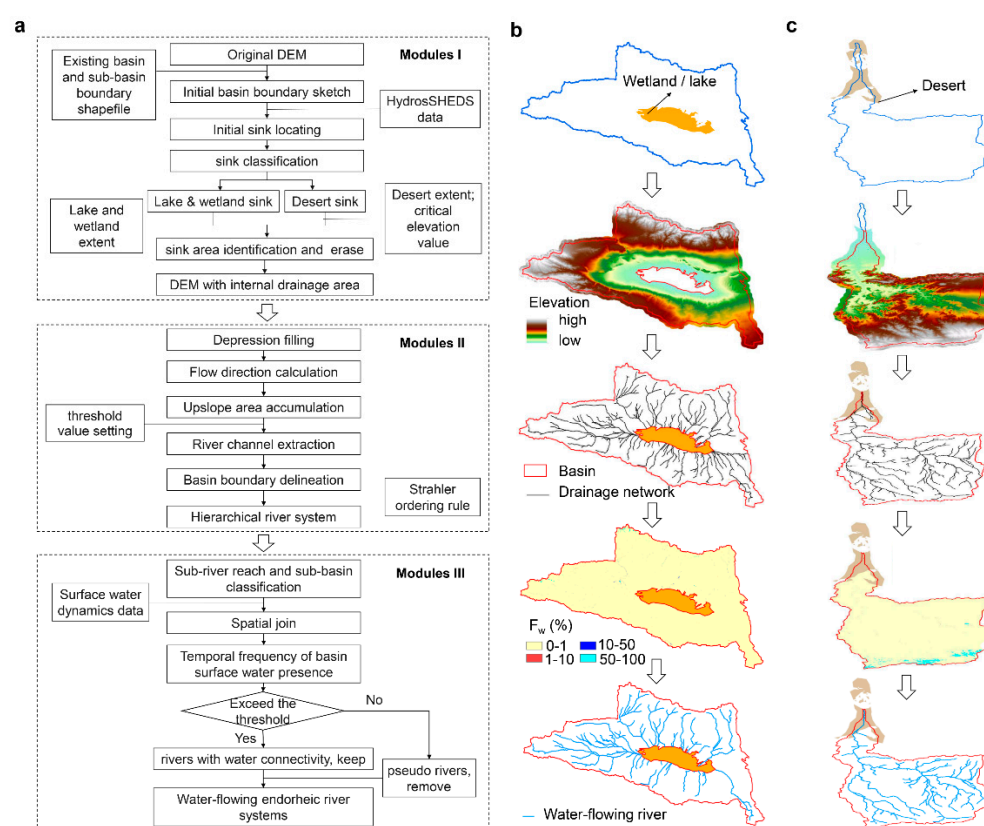


Figure 2. Identification of endorheic rivers. (a) The overall framework composed of three modules, i.e., introduction of internal drainage areas (Module I), extraction of river networks and delineation of basin boundaries (Module II), and identification of flowing rivers (Module III). (b,c) Separately represent two cases about the workflows on identification of endorheic rivers with a wet/lake sink and with a desert sink.

2.3.1. Introduction of Internal Drainage Areas

To guarantee the smooth carry out of endorheic river extraction, some pretreatment was undertaken whereby internal drainage areas were introduced (Module I).

Three types of sinks were observed in endorheic basins, i.e., lakes, wetlands, and desert areas. For each of endorheic river systems, the basin boundaries could be initially sketched out based on the basin or sub-basin boundaries information stored in HydroBASINS database (slightly expanding to the outside of the ridge line to guarantee the accurate extraction) as well as the elevation information (Figure 2b,c).

For both lake-draining basins and wetland-draining basins, the sink locations were initially identified based on the river networks information of HydroSHEDS database (in

the database sinks are processed as the junction nodes of multiple rivers). Lake sinks boundaries (referring those lakes without apparent outlets) were further identified by overlaying lakes information from the HydroLAKES Database on the DEM, while wetland sinks boundaries were identified by overlaying information from the wetlands information (corresponding to cell values 7–12) from global lake and wetland database (GLWD) on the DEM (Figure 2b).

The remaining rivers were considered to end in the desert. For these basins, we determined the sink location by visually examining with desert extent and elevation value (Figure 2c). A critical elevation value was set, below which a region was a sink. We then used Arc info to erase the pixels of sink area; thus, the outlets of water flow were created for the endorheic river systems.

2.3.2. Extraction of River Networks and Delineation of Basin Boundaries

Endorheic drainage networks were extracted using a high-efficiency algorithm based on a size-balanced binary search tree (Module II) [43]. Two threshold values (i.e., critical source area (number of grid cells) and local slope) in this study were involved during the extraction procedure, which were separately determined as 20 and 0.01. The stream-orders of rivers were defined by Strahler ordering scheme [44,45], where the first-order streams are headwaters without bifurcation, and the stream-order of downstream river at a confluence followed the rules as below:

$$n_d = \{n_1 + 1, n_1 = n_2; \max(n_1, n_2), n_1 \neq n_2\} \quad (1)$$

where n_d is the stream-order of the downstream river. n_1 and n_2 are the stream-orders of the upstream rivers at the confluence, respectively.

2.3.3. Identification of Flowing Rivers

Flowing endorheic river systems were identified by excluding the pseudo-rivers never carrying water flow (Module III). A pseudo-river identification hypothesis was proposed as follow: a pseudo-river was defined as a river channel never carrying water flow and was located in a river basin whose temporal frequency of surface water presence (set as F_w , %) during 1981–2015 was zero [20]. Information on surface water dynamic could be derived from satellite imagery [37]. A final check was conducted during which rivers erroneously identified as pseudo-rivers was manually modified (vice versa).

2.4. Characterization of River Networks

River networks were described from both the topological and geometric perspectives.

2.4.1. Test of the Horton Self-Similarity and Estimation of Horton Ratios

The river network followed some laws during its development [46], expressed as:

$$N_w = R_B^{N-w} \quad (2)$$

$$L_w = L_1 \times R_L^{w-1} \quad (3)$$

where is the stream-order. N_w and L_w are the total number and mean channel length of rivers at the w -order, respectively. R_B , and R_L , respectively indicate the proportionality between the channels number and channel length of one stream-order and those of a higher-order, are named as the bifurcation ratio and channel length ratio, and are collectively called the Horton ratios.

The Horton self-similarity of river networks stated constant Horton ratios at an appropriate range of stream-orders and can be tested through best linear interpolation:

$$\lg N_w = -(\lg R_B) \times w + N \times \lg R_B \quad (4)$$

$$\lg L_w = (\lg R_L) \times w + \lg L_1 - \lg R_L \quad (5)$$

A river network will be considered to be self-similar when the respective coefficient of determination R^2 is above a predefined value R_0^2 .

The Horton ratios were estimated as 10^b (Method I), where b is the slope of the best least squares fit to the above lineal modes [47].

An alternative method to estimate Horton ratios [47], called as the Average Method (II), is expressed as:

$$R_B = [(N_1/N_2) + (N_2/N_3) + \dots \dots + (N_{r-1}/N_r)]/(r - 1) \quad (6)$$

$$R_L = [(L_2/L_1) + (L_3/L_2) + \dots \dots + (L_r/L_{r-1})]/(r - 1) \quad (7)$$

where r is the upper limit of stream-order in which the Horton ratios exhibit convergence.

2.4.2. Calculation of Fractal Dimension

Based on the R_B , and R_L , we could further calculate the fractal dimension index (F_D) of river networks [48]:

$$F_D = \max(1, \log R_B / \log R_L) \quad (8)$$

F_D was an effective measure of river network and watershed topographic features. A greater F_D (e.g., >1.6) usually represented a more complicated river network and a more developed stage of geomorphologic evolutions [49].

2.4.3. Assessment of Drainage Density

We also introduced the drainage density (D_D), defined as the ratio of total channel length in a catchment to total catchment area, to measure the development level of rivers in the endorheic river basins [50]. In this study, we also made a hierarchal analysis on D_D .

For a river basin whose maximum stream-order is of N , the D_D at certain stream-orders could be calculated as below:

$$D_{D-w} = TL_w / A_w \quad (9)$$

where TL_w is the total length of rivers from 1- to w -order. A_w is the total catchment areas of rivers at w -order.

2.5. Quantification of Basin Properties

Basin characteristics were described through three dimensions by typical variables, as displayed in Table 1.

Table 1. List of variables as descriptors of river basin properties.

Category	Attribute	Abbreviation	Unit
Climate and Meteorology	Annual mean precipitation	P_{mean}	$\text{mm} \cdot \text{a}^{-1}$
	Monthly minimum precipitation	P_{min}	$\text{mm} \cdot \text{a}^{-1}$
	Monthly maximum precipitation	P_{max}	$\text{mm} \cdot \text{a}^{-1}$
	Potential evapotranspiration	PET	$\text{mm} \cdot \text{day}^{-1}$
	Annual mean actual evapotranspiration	T_{mean}	$^{\circ}\text{C}$
	Monthly minimum temperature	T_{min}	$^{\circ}\text{C}$
	Monthly maximum temperature	T_{max}	$^{\circ}\text{C}$
	Aridity index	AI	-
	Annual mean actual evapotranspiration	AET_{mean}	$\text{mm} \cdot \text{day}^{-1}$
	Monthly minimum actual evapotranspiration	AET_{min}	$\text{mm} \cdot \text{day}^{-1}$
	Monthly maximum actual evapotranspiration	AET_{max}	$\text{mm} \cdot \text{day}^{-1}$

Table 1. Cont.

Category	Attribute	Abbreviation	Unit
Hydrology and hydrogeology	Land surface runoff	R	mm
	Annual mean soil water content	SWC _{mean}	mm·a ⁻¹
	Monthly minimum soil water content	SWC _{min}	mm·a ⁻¹
	Monthly maximum soil water content	SWC _{max}	mm·a ⁻¹
	Groundwater type	GWT	-
Geomorphology	Mean basin slope	S	°
	Area proportion of glacier	Glacier	%
	Area proportion of oasis	Oasis	%
	Area proportion of vegetation	VC	%
	Area proportion of desert	Desert	%

2.6. Statistical Analysis

Relationships between hierarchical characteristics of river networks and primary basin factors were identified with Spearman correlation analysis (a value of $p < 0.01$ was considered significant). The relative importance of multiple basin factors to structural characteristics of endorheic rivers was estimated by using the multiple regression model (lm function in “stats” package in R) and variance decomposition analysis (calc. relimp function in the “relaimpo” package in R). The dissimilarities of structural parameters between the Tarim the Yellow River were examined by Wilcoxon rank-sum tests (wilcox.test function in “stats” package in R).

3. Results

3.1. Self-Similarity of Endorheic Rivers

The Horton self-similarity test was made for each river network identified from 60 representative sub-basins in the Tarim Basin. Figure 3 shows the distribution of p values and coefficient of determination (R^2). Based on the acceptance thresholds ($R^2 > 80\%$ and ANOVA p values < 0.05) for Horton self-similarity assumption [47], 83% and 73% of examined sub-basins pass the test in terms of R_B and R_L , respectively, suggesting that most endorheic river systems in the Tarim Basin could be considered as self-similar statistically.

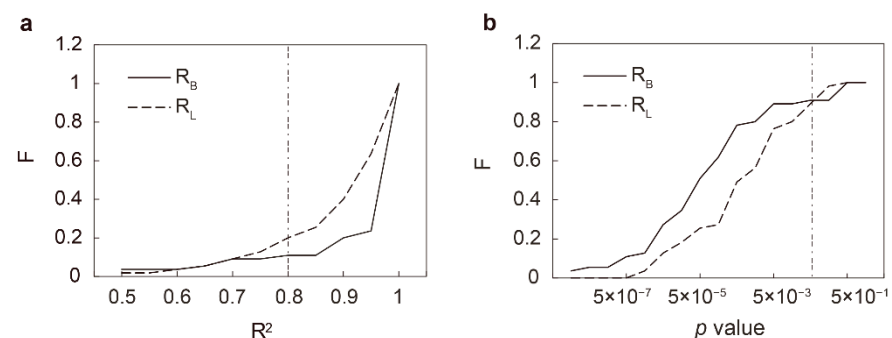


Figure 3. Distributions of river network parameters for endorheic sub-basins considered. Empirical cumulative distribution function of (a) the coefficients of determination, R^2 , and (b) the p value obtained during self-similarity test. F in (a,b) refers to the frequency of sub-basins whose R^2 or p do not exceeding a certain value.

To detect hierarchal characteristics of endorheic river structure, Figure 4 displays variations of four typical structural parameters (R_B , R_L , F_D , and D_D) as functions of stream-orders for representative sub-basins in the Tarim River basin. Convergences of R_B and R_L generally happen to rivers at stream-orders 1–4 (Figure 4a,b). As the stream-order increases from 5 to 7, R_B and R_L exhibit increased uncertainty. D_D remains stable with median values ranged 0.7–1.3 km⁻¹ at stream-orders 1–4, showing a sharp drop at Strahler order 5, and decreasing significantly with stream-orders after (Figure 4d).

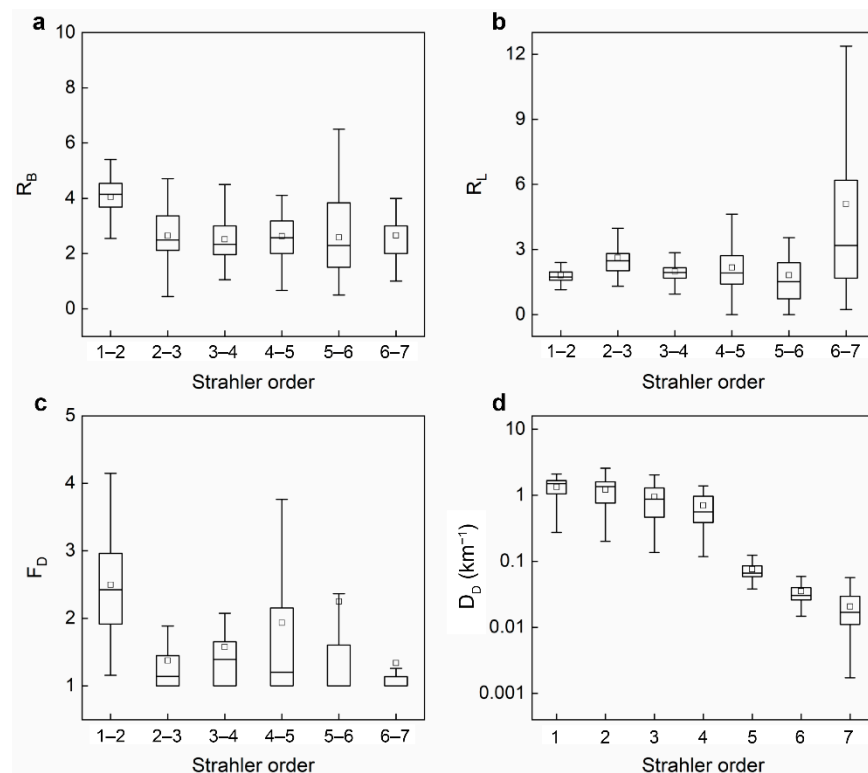


Figure 4. Structural parameters with different Strahler orders for river networks in the Tarim Basin: (a) bifurcation ratio (R_B), (b) channel length ratio (R_L), (c) fractal dimension index (F_D), and (d) drainage density (D_D , km^{-1}).

Overall, the self-similarity is fairly presented in about 70–80% of sub-basins in the Tarim, primarily at stream-orders 1–4. Such a topological rule could not be maintained for rivers at higher Strahler orders (>4) owing to very limited stream power to maintain the similar aggregation of rivers in the arid endorheic regions. Greater R_B and F_D with median values of 4.1 and 2.4 are presented at Strahler-orders 1–2, suggesting maintenance of dendritic structure in headwater streams (Figure 4a,c). Moreover, all the structure parameters show notable variations at stream-order 5, which might be related to local conditions of hydrogeology and geomorphology.

3.2. Structural Characteristics of Endorheic Rivers

For endorheic rivers passed the Horton self-similarity test, we estimated the Horton ratios (R_B , R_L) and F_D by regression method (I) and average method (II) and compared them by introducing a diagonal line representing ‘ $y = x$ ’ (Figure 5a–c). These two methods should be equally effective as most plots are distributed around the diagonal lines, and thus the ranges of Horton values ($R_B \in [1.6, 4.2]$, $R_L \in [1.6, 3.0]$) derived from the methods would not vary significantly, though both were lower than those typically observed in exohreic rivers [51], i.e., $R_B \in [3, 5]$, $R_L \in [1.5, 3.5]$. Similarly, about 80% of concerned sub-basins show a smaller F_D than that (1.6) are commonly observed in exohreic rivers [49,52].

Figure 5d shows the frequency histograms of drainage density (D_D , km^{-1}) for sub-basins. D_D ranges from 0.003 to 1.1 km^{-1} , which is also much lower than those (0.76–1.29 km^{-1}) computed for exohreic rivers at similar levels of basin scales in the humid and semi-arid regions [26].

Overall, endorheic rivers demonstrate lower R_B , R_L , F_D , and D_D in representative sub-basins in the Tarim compared with those derived from exohreic rivers at similar scales, which suggests less branching, undeveloped, and sparser river networks in endorheic basins.

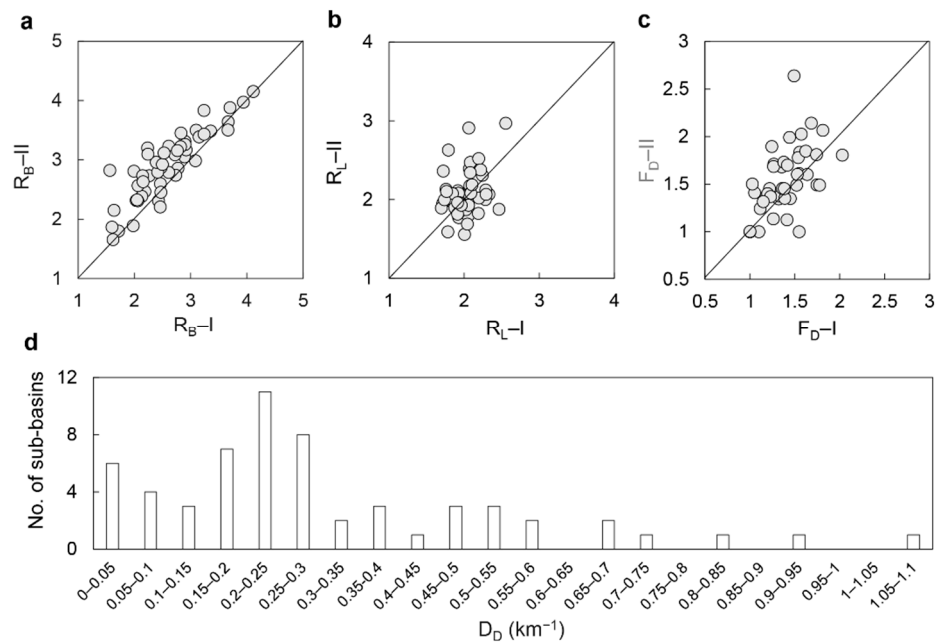


Figure 5. Distributions of river network parameters for endorheic sub-basins considered. Parameter space of (a) R_B , (b) R_L , and (c) fractal dimension index (F_D) estimated by regression method (I) and average method (II). (d) Frequency histograms of drainage density (D_D , km^{-1}).

3.3. Major Drivers of Endorheic River Structures

To investigate the primary influencing factors of endorheic river networks, we made a correlation analysis between structural parameters (R_B , F_D , D_D , and mean river length at stream-order 5 (L_5)) and 12 basin factors (Table 1) categorized into three major issues (climate and meteorology, hydrology and hydrogeology, geomorphology).

As results, there are 14, 15, 18, and 15 factors significantly correlated to R_B , F_D , D_D , and L_5 , respectively. Among the climatic and meteorological factors, the structural parameters of endorheic rivers in the Tarim Basin are mostly sensitive to potential evapotranspiration (PET) induced by high temperature and extra-terrestrial radiation. In Figure 6a–c, R_B , F_D , and D_D are all significantly negatively correlated to PET, with correlation coefficients in the range $-0.63 \sim -0.81$. However, a positive correlation is shown between the mean length of the 5-order rivers (L_5) and PET (Figure 6d). These results are reasonable since the high potential evaporation exacerbates the loss of surface runoff, leading to less stream power to sustain the river networks. Another important driving force in shaping river network would be the aridity index (AI), which is defined as the ratio of precipitation and PET. Extremely high potential evapotranspiration in the arid regions of Northwest China, together with scarce precipitation, in turn increase climate-induced aridity and facilitate extensive drying out of channels. Consequently, R_B , F_D , and D_D exhibit positive correlation with AI, while L_5 exhibits negative correlation with AI (Figure 6a–d). Actual evapotranspiration (AET) is the effective water quantity that is removed from the soil due to evaporation and transpiration processes. In the arid regions, AET is largely dependent on quantity of water available in the soil, hydrological properties, and vegetation characteristics, such as soil moisture, precipitation, and vegetation coverage, which are beneficial to the development of river networks and streamflow generations. Hence, positive correlations between AET_{\max} and R_B , F_D , and D_D are observed.

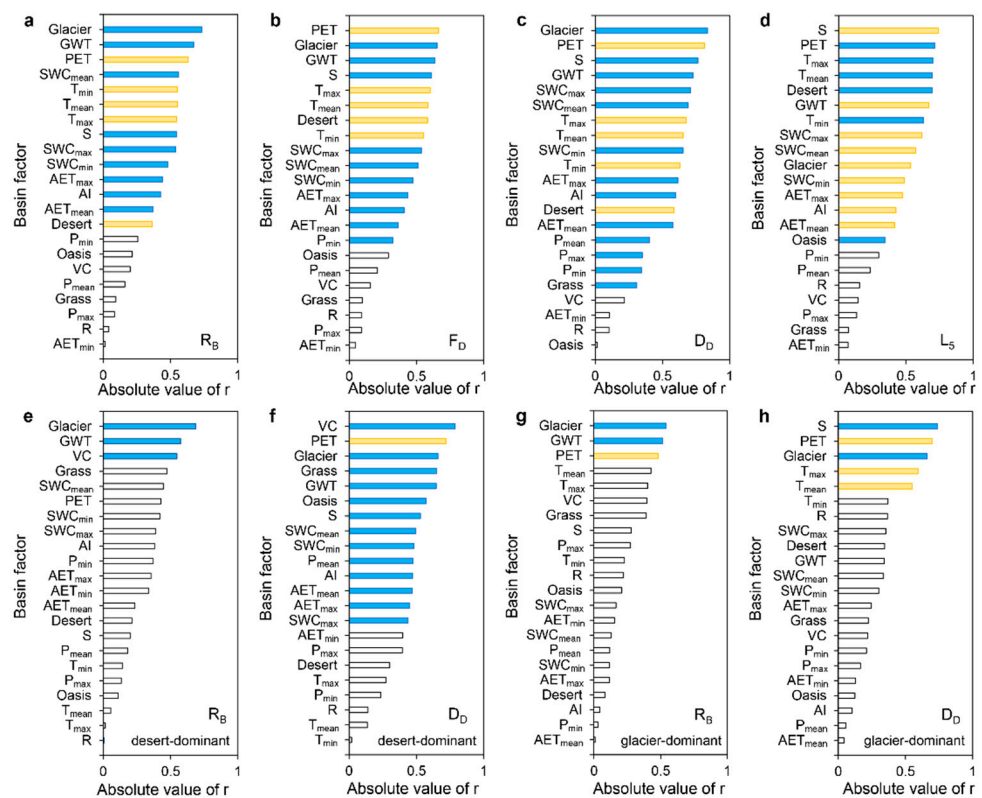


Figure 6. Correlation between structure parameters of endorheic rivers and basin factors. Spearman correlation coefficient (r) of: (a) bifurcation ratio (R_B); (b) fractal dimension (F_D); (c) drainage density (D_D); (d) mean length of the rivers at stream-order 5 (L_5) for the 60 sub-basins in the Tarim River basin. (e,f) are r values for desert-dominant sub-basins. (g,h) are the r values for glacier-dominant sub-basins. The blue and yellow histograms, respectively, represent significantly positive and negative correlations, whereas the white histogram represents no correlation observed.

Geomorphologic conditions, which could be described from perspectives of topography and underlying surface, are essential in characterizing the structural characteristics of endorheic rivers in the Tarim. In particular, the structural parameters are highly dependent on the basin slope (S), suggesting the key role of energy gradient in shaping river networks. Moreover, basin underlying surface conditions can also impact the structural properties of river networks. In the Tarim River basin, glacier and desert are two important basin underlying surface types. It appears that R_B , F_D , and D_D are positively correlated to the glacier extent (Glacier, %) and negatively correlated to desert extent (Desert, %), which is reasonable since the glacier is regarded as the key water source (glacier melt water) for endorheic rivers, and the desert could represent the scarcity of vegetation coverage and groundwater resources availability in the endorheic river basins.

Hydro-geological features are also found closely associated with endorheic river structures. For most endorheic basins with independent hydrological cycle systems in the Tarim River basin, endorheic rivers flow through five hydrogeological units in sequence from the watershed divide to the downstream direction, each corresponding to a specific groundwater type (Appendix A.1, Figure A1). In the high mountain areas (attitude above 3500–4000 m) where glacial permafrost is distributed, groundwater mainly exists as water above frozen layer (I), supplied by precipitation and melting water of snow and glacial. With large elevation gradient, groundwater would like to discharge into the gullies in the form of descending springs at appropriate locations, resulting in surface flow occurrence. In the middle and low mountainous areas (attitude below 3500 m), groundwater exists in the form of Karst water as well as fissure water in rocks, including cave water in Karst rocks (II), fissure water in metamorphic rocks, igneous rocks, and clastic rocks in mountains (III). Further downstream, pore water in loose soils is developed, including pore water

in alluvial and flooding layers in piedmont plains (IV) and pore water in sand dunes in deserts (V). Here, we introduce a groundwater type index (GWT), which is closely related to the groundwater type I, IV, and V, to represent the characteristics of hydrogeological units. We find an increasing trend in R_B , F_D , and D_D , and a decreasing trend in L_5 with increase of GWT. The decreased trend of streamflow occurrence frequency in rivers along the downstream dimension (Appendix A.1, Figure A1) further suggests that spatial distributions of hydrogeological units as well as groundwater types are well projected to the longitudinal patterns of surface flow intermittence, and therefore structural characteristics of endorheic rivers. Moreover, R_B , F_D , and D_D all show significant positive correlations with SWC_{max} , and L_5 exhibits significant negative correlation with SWC_{max} . These results suggest that the spatial distributions of hydrogeological units as well as groundwater types are closely related to the structural characteristics of endorheic rivers owing to the very tight hydraulic connection of surface water and groundwater in the endorheic regions that results from the frequent transformation between each of them.

The major drivers for structures of river networks vary among the 60 sub-basins in the Tarim with different underlying surface conditions. Two representative types of sub-basins could be identified, i.e., glacier-dominant river basin and desert-dominant river basin (Figure 1). The glacier-dominant rivers are those with greater glacier extent, usually flowing through high mountain areas, corresponding to hydrogeological units where groundwater mainly exists as water above frozen layer (I), supplied by precipitation and melting water of snow and glacial. Meanwhile, these rivers usually exhibit higher SWC and vegetation coverage. On the other hand, the desert-dominant rivers are those with greater desert proportion, usually distributed in flatter areas where pore water in loose soils (IV, V) is developed, and exhibit lower SWC and vegetation coverage. In the desert-dominant sub-basins, the vegetation coverage, grass, and oasis extent is found to be closely related to the structure of river networks, in addition to the glacier extent and groundwater type (Figure 6e,f). In the glacier-dominant sub-basins, PET is still the dominant factor, since the glacier melt water is sensitive to the temperature variation (Figure 6g,h).

Considering the correlations among the basin factors, we further use the multiple regression model and variance decomposition analysis to assess the relative importance of multiple basin factors to structure parameters of endorheic rivers (Figure 7). It appears that Glacier and PET explain the most of the R_B and F_D variance, while the Glacier and GWT are the most important drivers of D_D . L_5 , on the other hand, is mainly explained by Desert extent and temperature.

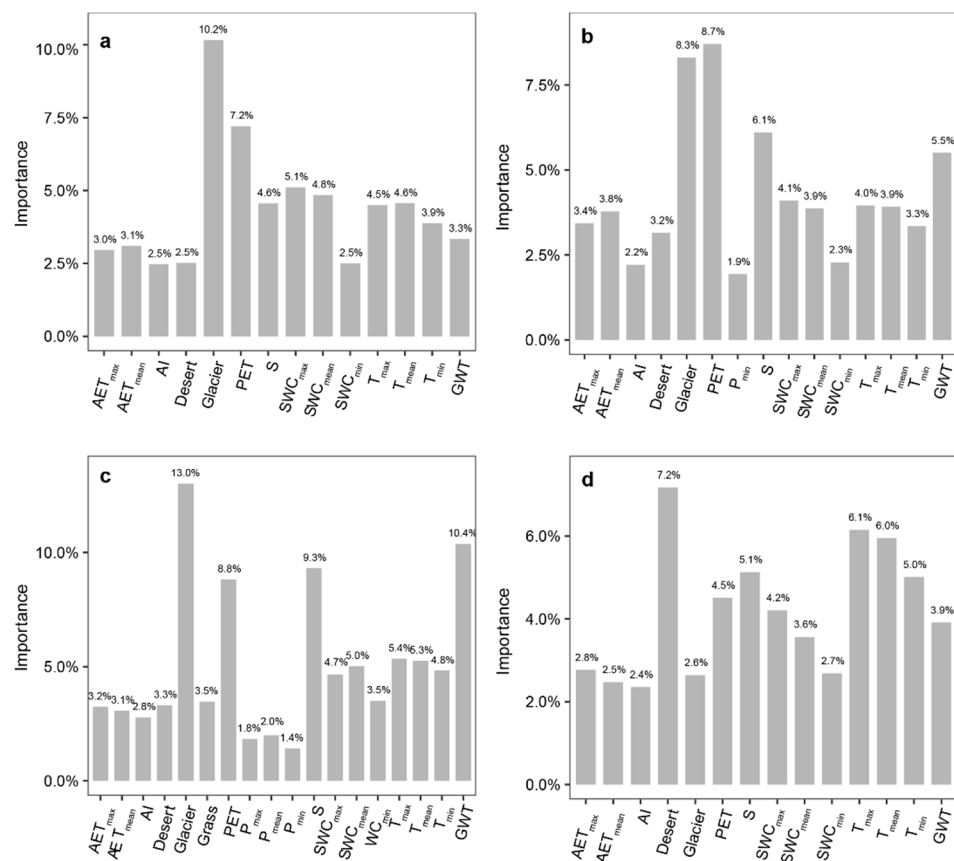


Figure 7. Relative contributions of basin factors to the differences in structural parameters for the 60 sub-basins in the Tarim River basin: (a) bifurcation ratio (R_B); (b) fractal dimension (F_D); (c) drainage density (D_D); (d) mean length of the rivers at stream-order 5 (L_5). The bar chart shows the variable importance, that is, the proportion of explained variability calculated via multiple regression modeling and variance decomposition analysis.

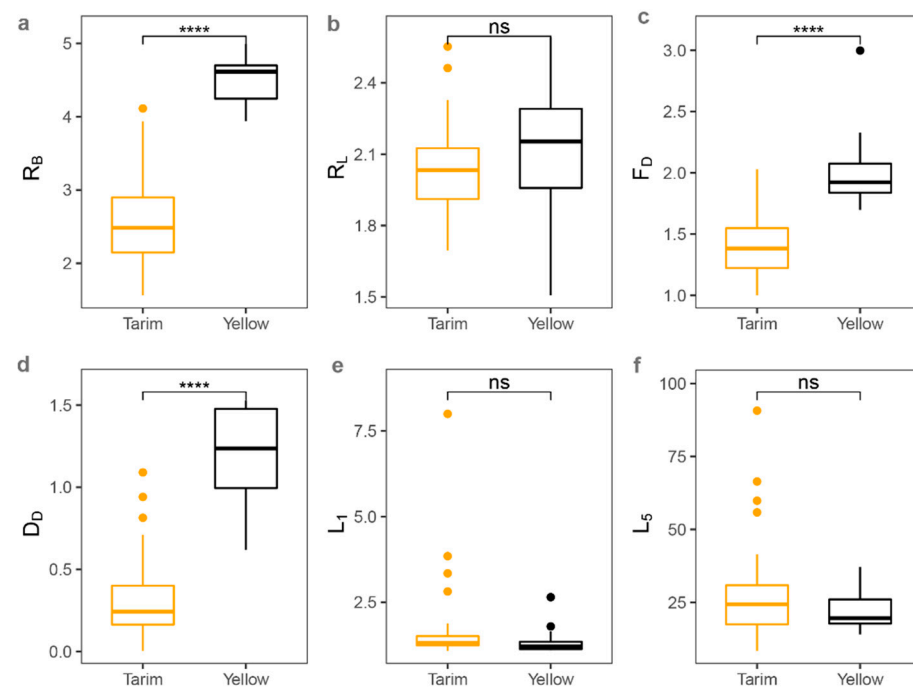
4. Discussion

4.1. Differences in Intrinsic Structures and Extrinsic Drivers of Endorheic and Exorheic Rivers

In the Tarim River basin, endorheic rivers exhibit a self-similarity only in the range of stream-orders 1–4, which is lower than the range of stream-orders 1–5 observed in exorheic rivers [26]. Compared the structural parameters of river networks in the Tarim and the Yellow River basins (Table 2), we find that median values of mean river length at Strahler order 1 (L_1) and 5 (L_5) are considerably larger in the former, while R_B , R_L , F_D , and D_D are greater in the latter. Moreover, we examine the dissimilarities of structural parameters between Tarim and Yellow River basin by using the Wilcoxon rank-sum tests. As is illustrated in Figure 8, significant differences in R_B , F_D , and D_D between the two basins are observed, which further confirm the vulnerability of endorheic rivers characterized with less branching, imperfect developed, and sparser network structures. It should be noted that the multifractal spectra, composed with a sequence of generalized F_D with different scaling exponents, could be used for a more detailed description of internal fractal structure in river networks [53]. As an extension of F_D , significant distinction of multifractal spectra between the endorheic and exorheic rivers could also be expected and worth exploring in the following analysis.

Table 2. Structural parameters of river networks in the Tarim and the Yellow River basins.

River Basin	Structural Parameter	Median Value
Tarim	R_B	2.48
	R_L	2.03
	F_D	1.38
	D_D	0.24 km^{-1}
	L_1	1.31 km
	L_5	24.35 km
Yellow	R_B	4.61
	R_L	2.15
	F_D	1.92
	D_D	1.24 km^{-1}
	L_1	1.21 km
	L_5	19.58 km

**Figure 8.** Comparison of structural parameters between the Tarim River and the Yellow River (ns, $p > 0.05$; **** $p < 0.0001$; Wilcoxon rank-sum test): (a) bifurcation ratio (R_B); (b) channel length ratio (R_L); (c) fractal dimension (F_D); (d) drainage density (D_D); (e) mean length of the rivers at stream-order 1 (L_1); (f) mean length of the rivers at stream-order 5 (L_5).

We further plotted relationships between structural parameters and key basin factors for sub-basins of the Tarim (Figure 9). For comparison, we displayed the results of 20 sub-basins at a similar scale in the Yellow River (Appendix A.2, Figure A2), which cover typical climatic and geomorphic conditions in the basin. We selected the Yellow River as a reference because the basin is partially located in the semi-arid regions, where it exhibits to a certain extent similar climatic and meteorological, hydrological, hydro-geologic, landform, and vegetation coverage conditions with the Tarim River basin. Differences in extrinsic drivers of endorheic and exorheic rivers are identified in terms of diverse river-basin relations.

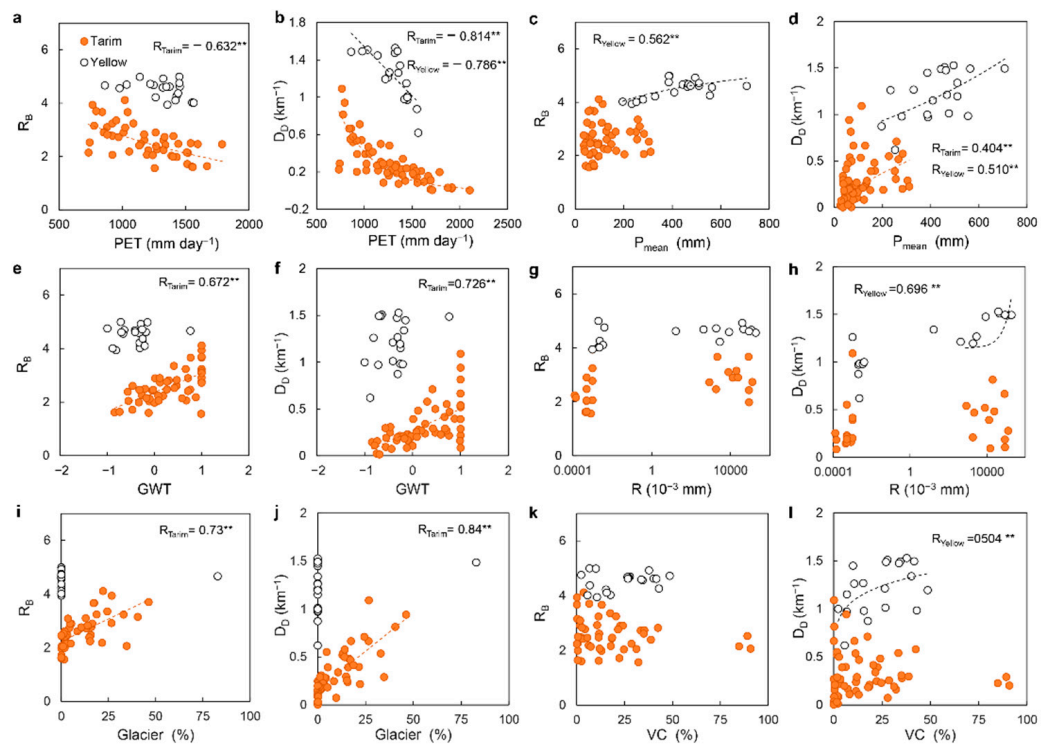


Figure 9. Relations between structural parameters (R_B , D_D) of river networks and basin factors including (a,b) PET, (c,d) P_{mean} , (e,f) GWT, (g,h) R, (i,j) Glacier, and (k,l) VC for representative sub-basins in the Tarim (orange dot) and the Yellow River basins (black hollow dot) (** $p < 0.01$; Spearman correlation).

River networks in the Tarim Basin are more sensitive to PET than those in the Yellow River basin, even though PET for sub-basins of the two basins are at similar levels (i.e., 733–2013 mm day⁻¹ in the Tarim, and 862–1564 mm day⁻¹ in the Yellow) (Figure 9a,b). For the Yellow River basin, structural parameters have much closer relations to precipitation, with R_B and D_D exhibiting significant positive feedback to increased P_{mean} (Figure 9c,d).

In sub-basins of the Tarim, groundwater mainly exists as water above frozen layer (I) with an area proportion of 41%, while the most common groundwater types are pore water in loose soils (groundwater type IV and V) with an area proportion of 43% (Figure 9e,f) in the sub-basins of the Yellow. For sub-basins in the Tarim River basin, R_B and D_D significantly increase with GWT. However, no correlation is found between structural parameters and GWT in the Yellow River basin. Alternatively, surface runoff (R) seems to be an important influencing factor of river networks in the Yellow River, even with comparable runoff of the Tarim (Figure 9g,h).

Compared the underlying surface condition of the two basins, we find that sub-basins in the Yellow mostly correspond to a relatively higher vegetation coverage (median VC = 27%) than sub-basins in the Tarim (median VC = 9%). Among the diverse surface underlying types in the Tarim River basin, glacier is widely distributed in 90% of concerned sub-basins, which significantly promotes both R_B and D_D of river networks. In the Yellow River basins, hierarchical characteristics of river networks are more closely related to vegetation cover in addition to the soil erodibility [26].

Overall, it appears that structure of endorheic networks is more related to the glacier extent, potential evapotranspiration, and groundwater type, which is essentially different from the structure of exorheic river represented by the Yellow River that is largely controlled by surface runoff, precipitation, and vegetation coverage.

4.2. Management Implications for Endorheic Rivers

Differentiated strategies are needed for sustainable management of varying kinds of endorheic rivers in fragile ecosystems. Commonly, a river is prone to sustaining streamflow when the channel has higher water supply and lower consumption [25]. For endorheic rivers in the Tarim, the streamflow is mainly supplied by glacial melt water, alpine precipitation, and release from existing water storage (e.g., groundwater, lakes), while consumption is mainly caused by the infiltration, evapotranspiration, and other natural and human-driven river discharge loss. Compared with exorheic rivers dominated by precipitation supply, the integrity and development degree of endorheic river networks are very sensitive to climatic factors. Hence, variation in PET and temperature should be focused as a matter of priority during the water resource management.

As a regulator for water resources, groundwater is important to maintenance of river surface hydraulic connections as well as ecosystem health in the endorheic river basin. In particular, changes in groundwater depth directly affect the soil moisture, vegetation growth, and land desertification. Therefore, local administrators need to put forward a scientific scheme for both annual total groundwater storage and groundwater level control, establish the integrated scheduling model of underground reservoir and surface water, and formulate the integrated management strategies for both surface runoff and groundwater regulation in the arid regions.

Considering the complex geomorphic dependence of endorheic river structure induced by multiple underlying surface types, specific strategies are highly necessary for watershed management in the endorheic regions. For the desert-dominant sub-basins, river networks are highly dependent to the vegetation coverage, grass, and oasis extent. In such a case, vegetation restoration strategies should be preferred options for watershed sustainable management. For the glacier-dominant sub-basins, the glacier melt water dynamic under climate change would be the key factor influencing flow regimes and integrity of endorheic rivers, which highlights the particular importance of adaptive policies against climate change.

5. Conclusions

Based on the river networks identified from DEMs and surface water dynamic information derived from satellite image in the Tarim River basin, we investigate the structural characteristics of endorheic rivers and their geomorphic and climatic dependence. Compared with exorheic rivers, endorheic rivers exhibit significant differences in the stream-order range of self-similarity, structural characteristics, and influencing factors. The lower stream power limits the capability of channel aggregation and narrows the range of stream-orders for self-similarity in endorheic river networks, leading 70~80% of the sub-basins in the Tarim to observe Horton's law within stream-orders 1–4. Moreover, the river networks exhibit lower R_B , R_L , F_D , and D_D in representative sub-basins of the Tarim, demonstrating sparser and imperfect developed branching river networks in endorheic regions. The structural parameters for endorheic rivers are more related to glacier extent ($r = 0.67\sim 0.84$), potential evapotranspiration ($r = 0.63\sim 0.81$), and groundwater type index ($r = 0.64\sim 0.73$), which is essentially different from the exorheic rivers like the Yellow River, which is largely controlled by surface runoff, precipitation, and vegetation coverage. This study provides new insights into topological structure of endorheic river networks and highlights the significance of differentiated strategies for sustainable river management of endorheic ecosystems sensitive to climate change.

Author Contributions: Conceptualization, J.N. and Y.W.; methodology, Y.W., D.L., and E.L.; software, Y.W.; validation, D.L. and E.L.; formal analysis, Y.W.; investigation, E.L.; data curation, E.L.; writing—original draft preparation, Y.W. and D.L.; writing—review and editing, Y.W. and J.N.; visualization, Y.W.; supervision, J.N. All authors have read and agreed to the published version of the manuscript.

Funding: This research was funded by the National Natural Science Foundation of China, grant number 52109075 and U2243201; and the Fundamental Research Funds for the Central Universities, grant number 2021NTST27.

Data Availability Statement: The data included in this study are available upon request from the corresponding author.

Conflicts of Interest: The authors declare no conflict of interest. The funders had no role in the design of the study; in the collection, analyses, or interpretation of data; in the writing of the manuscript, or in the decision to publish the results.

Appendix A.

Appendix A.1. Hydrogeological Conditions of the Tarim River Basin

This longitudinal flow frequency pattern of endorheic rivers is closely related to the hydrogeological features, which affect geological transitions along the channel as well as the gains and losses of groundwater along the channels. For most endorheic basins with independent hydrological cycle systems in the Tarim, endorheic rivers flow through five hydrogeological units along the downstream direction, each corresponding to a specific groundwater type (Figure A1). The streamflow intermittence of endorheic rivers varies with groundwater types. From groundwater type I to type V along the downstream dimension, the median values of temporal frequency of surface water presence (set as F_w , %) reduced from 2.2% to 0.4%. This result suggests that the spatial distributions of hydrogeological units as well as groundwater types are well projected to the longitudinal patterns of surface flow intermittence variations.

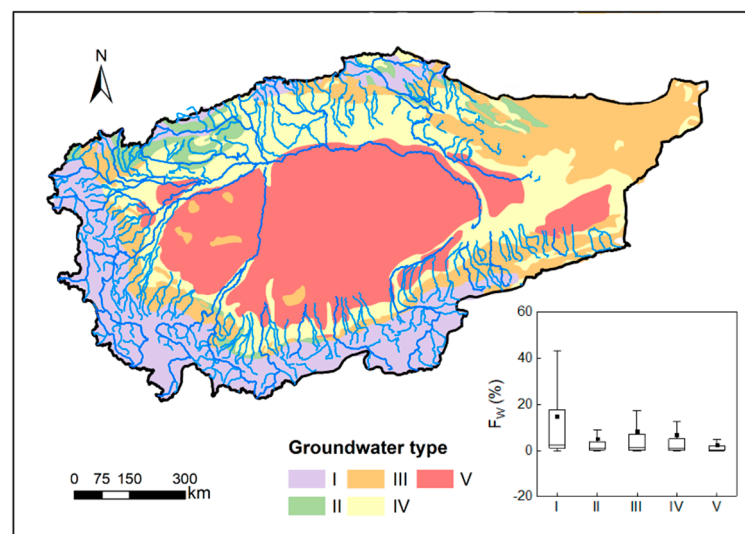


Figure A1. Hydrogeological unit map in the Tarim River basin classified by five major groundwater types, i.e., I, II, III, and IV, corresponding to water above frozen layer, cave water in Karst rocks, fissure water in rocks, pore water in loose soil, and sand dunes in deserts, respectively. The box plots illustrate the variation of streamflow occurrence frequency (F_w , %) in endorheic rivers flowing through different groundwater types.

Appendix A.2. Representative Sub-Basins in the Yellow River Basin

The Yellow River, with a total river length of 5,464 km, is the second longest river in China, with a total area of 758,600 km², and the basin is distributed in 95°E–119°E, 32°N–42°N, dominantly characterized by a semi-arid and arid climate. Flowing through world's largest and thickest loess deposits, the Yellow River has the largest average annual sediment yield (1.6×10^{12} kg/yr during 1919–1960) in the world.

For comparison, we selected 20 sub-basins in the Yellow River representing typical climatic and geomorphic conditions as illustrated in Figure A2. The selected sub-basins

have catchment areas in the range of 5474~38311 km². The maximum Strahler orders for river networks in the sub-basins range from 6 to 7.

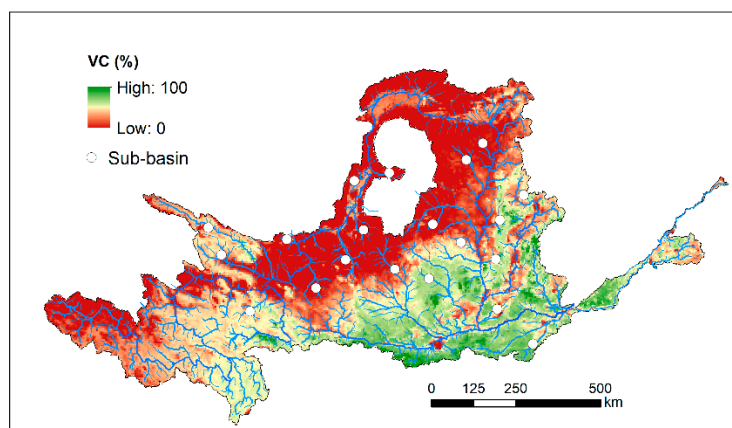


Figure A2. Vegetation coverage and distribution of 20 representative sub-basins in the Yellow River basin.

References

- Li, X.; Cheng, G.; Ge, Y.; Li, H.; Han, F.; Hu, X.; Tian, W.; Tian, Y.; Pan, X.; Nian, Y.; et al. Hydrological Cycle in the Heihe River Basin and Its Implication for Water Resource Management in Endorheic Basins. *J. Geophys. Res. Atmos.* **2018**, *123*, 890–914. [\[CrossRef\]](#)
- Li, Y.; Zhang, C.; Wang, N.; Han, Q.; Zhang, X.; Liu, Y.; Xu, L.; Ye, W. Substantial Inorganic Carbon Sink in Closed Drainage Basins Globally. *Nat. Geosci.* **2017**, *10*, 501–506. [\[CrossRef\]](#)
- Maasri, A.; Thorp, J.H.; Gelhaus, J.K.; Tromboni, F.; Chandra, S.; Kenner, S.J. Communities Associated with the Functional Process Zone Scale: A Case Study of Stream Macroinvertebrates in Endorheic Drainages. *Sci. Total Environ.* **2019**, *677*, 184–193. [\[CrossRef\]](#)
- Li, X.; Zhang, L.; Zheng, Y.; Yang, D.; Wu, F.; Tian, Y.; Han, F.; Gao, B.; Li, H.; Zhang, Y.; et al. Novel Hybrid Coupling of Ecohydrology and Socioeconomy at River Basin Scale: A Watershed System Model for the Heihe River Basin. *Environ. Model. Softw.* **2021**, *141*, 105058. [\[CrossRef\]](#)
- Pavelsky, T.M. World's Landlocked Basins Drying. *Nat. Geosci.* **2018**, *11*, 892–893. [\[CrossRef\]](#)
- Li, Z.; Chen, Y.; Fang, G.; Li, Y. Multivariate Assessment and Attribution of Droughts in Central Asia. *Sci. Rep.* **2017**, *7*, 1–12. [\[CrossRef\]](#)
- Messenger, M.L.; Lehner, B.; Cockburn, C.; Lamouroux, N.; Pella, H.; Snelder, T.; Tockner, K.; Trautmann, T.; Watt, C.; Datry, T. Global Prevalence of Non-Perennial Rivers and Streams. *Nature* **2021**, *594*, 391–397. [\[CrossRef\]](#)
- Yang, P.; Xia, J.; Zhan, C.; Qiao, Y.; Wang, Y. Monitoring the Spatio-Temporal Changes of Terrestrial Water Storage Using GRACE Data in the Tarim River Basin Between 2002 and 2015. *Sci. Total Environ.* **2017**, *595*, 218–228. [\[CrossRef\]](#)
- Wang, J.; Song, C.; Reager, J.T.; Yao, F.; Famiglietti, J.S.; Sheng, Y.; Macdonald, G.M.; Brun, F.; Schmied, H.M.; Marston, R.A.; et al. Recent Global Decline in Endorheic Basin Water Storages. *Nat. Geosci.* **2018**, *11*, 926–932. [\[CrossRef\]](#)
- Wang, W.; Chen, Y.; Wang, W. Groundwater Recharge in the Oasis-Desert Areas of Northern Tarim Basin, Northwest China. *Hydrol. Res.* **2020**, *51*, 1506–1520. [\[CrossRef\]](#)
- Lai, J.; Li, Y.; Chen, J.; Niu, G.-Y.; Lin, P.; Li, Q.; Wang, L.; Han, J.; Luo, Z.; Sun, Y. Massive Crop Expansion Threatens Agriculture and Water Sustainability in Northwestern China. *Environ. Res. Lett.* **2022**, *17*, 034003. [\[CrossRef\]](#)
- Rad, A.M.; Kreitler, J.; Abatzoglou, J.T.; Fallon, K.; Roche, K.R.; Sadegh, M. Anthropogenic Stressors Compound Climate Impacts on Inland Lake Dynamics: The Case of Hamun Lakes. *Sci. Total Environ.* **2022**, *829*, 154419. [\[CrossRef\]](#)
- Dorsaz, J.-M.; Gironás, J.; Escauriaza, C.; Rinaldo, A. The Geomorphometry of Endorheic Drainage Basins: Implications for Interpreting and Modelling Their Evolution. *Earth Surf. Process. Landforms* **2013**, *38*, 1881–1896. [\[CrossRef\]](#)
- Yapiyev, V.; Sagintayev, Z.; Inglezakis, V.J.; Samarkhanov, K.; Verhoef, A. Essentials of Endorheic Basins and Lakes: A Review in the Context of Current and Future Water Resource Management and Mitigation Activities in Central Asia. *Water* **2017**, *9*, 798. [\[CrossRef\]](#)
- Benstead, J.P.; Leigh, D.S. An Expanded Role for River Networks. *Nat. Geosci.* **2012**, *5*, 678–679. [\[CrossRef\]](#)
- Sauquet, E.; Shanfield, M.; Hammond, J.C.; Sefton, C.; Leigh, C.; Datry, T. Classification and Trends in Intermittent River Flow Regimes in Australia, Northwestern Europe and USA: A Global Perspective. *J. Hydrol.* **2021**, *597*, 126170. [\[CrossRef\]](#)
- Erdenee, B.; Maasri, A.; Gelhaus, J.K.; Hayford, B.L.; Thorp, J.H.; Kotlinski, N.E. Comparison of Streamflow Patterns in Drainages of Two Major Terminal Basins: The United States Great Basin and Mongolia's Central Asian Internal Drainage. *Inland Waters* **2021**, *11*, 368–380. [\[CrossRef\]](#)

18. Yan, D.; Li, M.; Bi, W.; Weng, B.; Qin, T.; Wang, J.; Do, P. A Data Set of Inland Lake Catchment Boundaries for the Qiangtang Plateau. *Sci. Data* **2019**, *6*, 62. [[CrossRef](#)]
19. Liu, K.; Song, C.; Ke, L.; Jiang, L.; Ma, R. Automatic Watershed Delineation in the Tibetan Endorheic Basin: A Lake-Oriented Approach Based on Digital Elevation Models. *Geomorphology* **2020**, *358*, 107127. [[CrossRef](#)]
20. Wang, Y.; Ni, J.; Yue, Y.; Li, J.; Borthwick, A.G.L.; Cai, X.; Xue, A.; Li, L.; Wang, G. Solving the Mystery of Vanishing Rivers in China. *Natl. Sci. Rev.* **2019**, *6*, 1239–1246. [[CrossRef](#)]
21. Sun, F.; Wang, Y.; Chen, Y.; Li, Y.; Zhang, Q.; Qin, J.; Kayumba, P. Historic and Simulated Desert-Oasis Ecotone Changes in the Arid Tarim River Basin, China. *Remote Sens.* **2021**, *13*, 647. [[CrossRef](#)]
22. Wang, H.; Wen, X.; Wang, Y.; Cai, L.; Peng, D.; Liu, Y. China's Land Cover Fraction Change during 2001–2015 Based on Remote Sensed Data Fusion between MCD12 and CCI-LC. *Remote Sens.* **2021**, *13*, 341. [[CrossRef](#)]
23. Wang, N.; Liu, W.; Wang, H.; Sun, F.; Duan, W.; Li, Z.; Li, Z.; Chen, Y. Improving Streamflow and Flood Simulations in Three Headwater Catchments of the Tarim River Based on a Coupled Glacier-Hydrological Model. *J. Hydrol.* **2021**, *603*, 127048. [[CrossRef](#)]
24. Wang, X.; Luo, Y.; Sun, L.; Shafeeque, M. Different Climate Factors Contributing for Runoff Increases in The High Glacierized Tributaries of Tarim River Basin, China. *J. Hydrol. Reg. Stud.* **2021**, *36*, 100845. [[CrossRef](#)]
25. Costigan, K.H.; Kennard, M.J.; Leigh, C.; Sauquet, E.; Detry, T.; Boulton, A.J. Flow Regimes in Intermittent Rivers and Ephemeral Streams. In *Intermittent Rivers and Ephemeral Streams*; Academic Press: Cambridge, MA, USA, 2017; pp. 51–78.
26. Chen, X.; Wang, Y.; Ni, J. Structural Characteristics of River Networks and Their Relations to Basin Factors in the Yangtze and Yellow River basins. *Sci. China Technol. Sci.* **2019**, *62*, 1885–1895. [[CrossRef](#)]
27. Perron, J.T.; Richardson, P.; Ferrier, K.; Lapotre, M. The Root of Branching River Networks. *Nature* **2012**, *492*, 100–103. [[CrossRef](#)]
28. Ranjbar, S.; Hooshyar, M.; Singh, A.; Wang, D. Quantifying Climatic Controls on River Network Branching Structure Across Scales. *Water Resour. Res.* **2018**, *54*, 7347–7360. [[CrossRef](#)]
29. Ni, J.; Wang, H.; Ma, T.; Huang, R.; Ciais, P.; Li, Z.; Yue, Y.; Chen, J.; Li, B.; Wang, Y.; et al. Three Gorges Dam: Friend or Foe of Riverine Greenhouse Gases? *Natl. Sci. Rev.* **2022**, *9*, nwac013. [[CrossRef](#)]
30. Wang, Y.; Chen, X.; Borthwick, A.G.L.; Li, T.; Liu, H.; Yang, S.; Zheng, C.; Xu, J.; Ni, J. Sustainability of Global Golden Inland Waterways. *Nat. Commun.* **2020**, *11*, 1553. [[CrossRef](#)]
31. Liu, K.; Ke, L.; Wang, J.; Jiang, L.; Richards, K.S.; Sheng, Y.; Zhu, Y.; Fan, C.; Zhan, P.; Luo, S.; et al. Ongoing Drainage Reorganization Driven by Rapid Lake Growths on the Tibetan Plateau. *Geophys. Res. Lett.* **2021**, *48*, e2021GL095795. [[CrossRef](#)]
32. Lu, S.; Jin, J.; Zhou, J.; Li, X.; Ju, J.; Li, M.; Chen, F.; Zhu, L.; Zhao, H.; Yan, Q.; et al. Drainage Basin Reorganization and Endorheic-Exorheic Transition Triggered by Climate Change and Human Intervention. *Glob. Planet. Chang.* **2021**, *201*, 103494. [[CrossRef](#)]
33. Xu, J.; Ling, H.; Zhang, G.; Yan, J.; Deng, M.; Wang, G.; Xu, S. Variations in the Dissolved Carbon Concentrations of the Shallow Groundwater in a Desert Inland River Basin. *J. Hydrol.* **2021**, *602*, 126774. [[CrossRef](#)]
34. Xing, Z.; Huang, H.; Li, Y.; Liu, S.; Wang, D.; Yuan, Y.; Zhao, Z.; Bu, L. Management of Sustainable Ecological Water Levels of Endorheic Salt Lakes in the Inner Mongolian Plateau of China Based on Eco-Hydrological Processes. *Hydrol. Process.* **2021**, *35*, e14192. [[CrossRef](#)]
35. Shen, Q.; Ma, Y. Did Water Diversion Projects Lead to Sustainable Ecological Restoration in Arid Endorheic Basins? Lessons From Long-Term Changes of Multiple Ecosystem Indicators in the lower Heihe River Basin. *Sci. Total Environ.* **2019**, *701*, 134785. [[CrossRef](#)] [[PubMed](#)]
36. Editorial Committee of Encyclopedia of Rivers and Lakes in China. *Encyclopedia of Rivers and Lakes in China*; China Waterpower Press: Beijing, China, 2014.
37. Pekel, J.-F.; Cottam, A.; Gorelick, N.; Belward, A.S. High-Resolution Mapping of Global Surface Water and Its Long-Term Changes. *Nature* **2016**, *540*, 418–422. [[CrossRef](#)]
38. Vaze, J.; Teng, J.; Spencer, G. Impact of DEM Accuracy and Resolution on Topographic Indices. *Environ. Model. Softw.* **2010**, *25*, 1086–1098. [[CrossRef](#)]
39. Hou, J.; Li, X.; Pan, Z.; Wang, J.; Wang, R. Effect of Digital Elevation Model Spatial Resolution on Depression Storage. *Hydrol. Process.* **2021**, *35*, e14381. [[CrossRef](#)]
40. Bernard, T.G.; Davy, P.; Lague, D. Hydro-Geomorphometric Metrics for High Resolution Fluvial Landscape Analysis. *J. Geophys. Res. Earth Surf.* **2022**, *127*, e2021JF006535. [[CrossRef](#)]
41. Costabile, P.; Costanzo, C.; Gandolfi, C.; Gangi, F.; Masseroni, D. Effects of DEM Depression Filling on River Drainage Patterns and Surface Runoff Generated by 2D Rain-on-Grid Scenarios. *Water* **2022**, *14*, 997. [[CrossRef](#)]
42. Costabile, P.; Costanzo, C. A 2D-SWEs Framework for Efficient Catchment-Scale Simulations: Hydrodynamic Scaling Properties of River Networks and Implications for Non-Uniform Grids Generation. *J. Hydrol.* **2021**, *599*, 126306. [[CrossRef](#)]
43. Bai, R.; Li, T.; Huang, Y.; Li, J.; Wang, G. An Efficient and Comprehensive Method for Drainage Network Extraction from DEM With Billions of Pixels Using a Size-Balanced Binary Search Tree. *Geomorphology* **2015**, *238*, 56–67. [[CrossRef](#)]
44. Strahler, A.N. Hypsometric (Area-Altitude) Analysis of Erosional Topography. *Geol. Soc. Am.* **1952**, *63*, 1117–1142. [[CrossRef](#)]
45. Strahler, A.N. Quantitative Analysis of Watershed Geomorphology. *Eos Trans. Am. Geophys. Union* **1957**, *38*, 913–920. [[CrossRef](#)]
46. Horton, R.E. Erosional Development of Streams and Their Drainage Basins: Hydro-Physical Approach to Quantitative Morphology. *Geol. Soc. Am. Bull.* **1945**, *56*, 275–370. [[CrossRef](#)]

47. Zanardo, S.; Zaliapin, I.; Foufoula-Georgiou, E. Are American Rivers Tokunaga Self-Similar? New Results on Fluvial Network Topology and Its Climatic Dependence. *J. Geophys. Res. Earth Surf.* **2013**, *118*, 166–183. [[CrossRef](#)]
48. Martinez, F.; Manriquez, H.; Ojeda, A.; Olea, G. Organization Patterns of Complex River Networks in Chile: A Fractal Morphology. *Mathematics* **2022**, *10*, 1806. [[CrossRef](#)]
49. He, L.H.; Zhao, H. The Fractal Dimension of River Networks and Its Interpretation. *Sci. Geogr. Sin.* **1996**, *16*, 124–128.
50. Collins, D.; Bras, R.L. Climatic and Ecological Controls of Equilibrium Drainage Density, Relief, and Channel Concavity in Dry Lands. *Water Resour. Res.* **2010**, *46*, W04508. [[CrossRef](#)]
51. Rui, X.F. *Principles of Hydrology*; China Water & Power Press: Beijing, China, 2004.
52. Wang, Y.C.; Gao, X.W.; Li, T.J.; Yue, Y.; Fang, H.Q.; Ni, J.R. Geocode-based Aquatic Habitats in Hierarchical System of the Yellow River Basin. *J. Environ. Informatics* **2018**, *32*, 69–81. [[CrossRef](#)]
53. Kusák, M. Application of Fractal and Multifractal Analysis on Blue Nile Drainage Patterns in the Morphostructural Analysis of the Ethiopian Highlands, Ethiopia. *Prog. Phys. Geogr. Earth Environ.* **2022**, *46*, 357–370. [[CrossRef](#)]